www.czasopisma.pan.pl PAN POLSKA AKADEMIA NAUK www.journals.pan.pl

Arch. Metall. Mater., Vol. 61 (2016), No 3, p. 1515–1520

DOI: 10.1515/amm-2016-0248

S. ISLAK*#, C. ÖZORAK*, C. T. SEZGIN**, M. AKKAŞ**

EFFECT OF BORON ON MICROSTRUCTURE AND MICROHARDNESS PROPERTIES OF MO-SI-B BASED COATINGS PRODUCED VIA TIG PROCESS

In this study, Mo-Si-B based coatings were produced using tungsten inert gas (TIG) process on the medium carbon steel because the physical, chemical, and mechanical properties of these alloys are particularly favourable for high-temperature structural applications. It is aimed to investigate of microstructure and microhardness properties of Mo-Si-B based coatings. Optical microscopy (OM), X-ray diffraction (XRD) and scanning electron microscopy (SEM) were used to characterize the microstructures of Mo-Si-B based coatings. The XRD results showed that microstructure of Mo–Si–B coating consists of α-Mo, α-Fe, Mo2B, Mo3Si and Mo5SiB2 phases. It was reported that the grains in the microstructure were finer with increasing amounts of boron which caused to occur phase precipitations in the grain boundary. Besides, the average microhardness of coatings changed between 735 HV0.3 and 1140 HV0.3 depending on boron content.

Keywords: Mo-Si-B coating, microstructure, microhardness, TIG

1. Introduction

In the areas such as power generation and aerospace, Ni-based super-alloys have reached their physical limits in terms of their maximum operational condition temperature (1200 °C), which is already approaching 90% of its melting point [1]. Nowadays, Mo-Si-B alloys are extremely popular materials for high temperature applications. Because molybdenum based materials have some characteristic properties such as high melting point, high strength, creep strength and oxidation resistance, these alloys are widely used in the aforementioned applications. MoxSiy is a binary alloy refractory compound and therefore it has excellent strength at high temperatures [2-3].

Mo-Si-B are used to coat many metals which are used at the high temperature without any oxidation. Molybdenum-based systems have a relatively high density and marginal ductility, and, for low Si and B concentrations, they suffer from poor oxidation resistance. Precious metal super alloys exhibit very high densities and are very expensive. Mo_3Si exhibits the A15 crystal structure and it is brittle. Mo_5SiB_2 (T2) exhibits a tetragonal crystal structure with the Cr_5B_3 structure type, with 32 atoms in the unit cell; like Mo_3Si, it is brittle [4]. The fracture toughness of the Mo-Si-B alloy at room temperature has low toughness (8 MPa). But toughness increases gradually with temperature (17-18 MPa at 1200 °C, 25 MPa at 1400 °C) [5]. B-doped Mo5Si3 shows excellent oxidation resistance at temperatures ranging in the air. The excellent oxidation resistance is considered to be formed of a continuous and non-porous oxide (borosilicate glass) scale [6]. In contrast, B-undoped Mo_5Si_3 forms porous.

Researchers are using different methods for Mo-Si-B coatings such as spark plasma sintering, atmospheric plasma sintering, mechanical alloying, pack cementation process, plasma spray etc. [7-8]. There is no study on the production of Mo-Si-B coatings by tungsten inert gas (TIG) surfacing process. TIG surfacing process is a cost-effective approach which is applied when reactive materials (as coatings or substrates) are involved. In this method, substrate surface and powder or hard filler wire used for coating were melted down using arc source and then solidified, which resulted in the formation of a new composite layer [9-10]. Because of all these advantages of the TIG method, the objective of the present work is to produce the Mo–Si–B coating on the medium carbon steel and investigate the microstructure and microhardness of the coating.

2. Experimental studies

The powder mixture of Mo, Si and B was prepared according to Table 1 in order to observe the effect of boron addition Mo-Si alloy and to obtain Mo_5Si_2 (T2) phase. These alloys were produced on AISI 1040 steel with dimensions 100 mm×15 mm×10 mm using tungsten inert gas (TIG) surfacing process. The operating principle of TIG process system is schematically shown in Fig. 1.

The TIG process parameters which were used in this research are listed as follows: working voltage 20 V, working current 160 A, the travel speed of the nozzle 72 mm/min, the shielding gas flux (Ar) 12 L/min, electrode type W-%2 ThO_2 and the electrode diameter is 2.4 mm. Before TIG surfacing process, surfaces of substrate material were cleaned with acetone. Because the shielding gas didn't remove powders

* KASTAMONU UNIVERSITY, FACULTY OF ENGINEERING AND ARCHITECTURE, DEPARTMENT OF MATERIALS SCIENCE AND NANOTECHNOLOGY ENGINEERING, KASTAMONU, TURKEY

** KASTAMONU UNIVERSITY, CIDE RIFAT ILGAZ VOCATIONAL HIGH SCHOOL, KASTAMONU, TURKEY

Corresponding author: serkan@kastamonu.edu.tr

TABLE 1

Compositions of powder mixture

Composition number	Mo		Si		B	
	wt%	at%	wt%	at%	wt%	at%
1	95	85	5	15	0	0
2	94	78.5	5	14.5	1	7
3	93	73.5	5	13.5	2	13
4	92	68.5	5	12.5	3	19
5	91	64	5	12	4	24

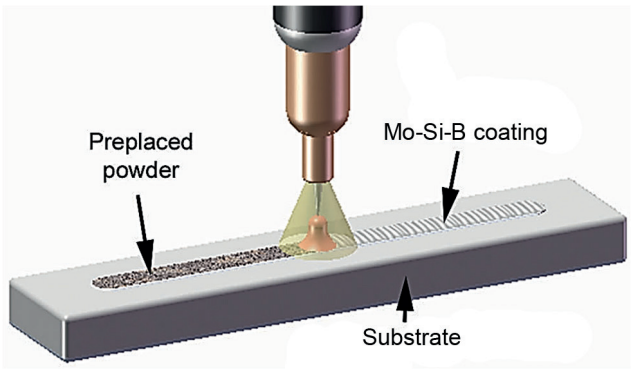

Fig. 1. Schematic diagram of the TIG process system

from the surface of substrate, powders were placed on to substrate after being mixed with a little amount of binder. Then, samples were dried at 50 °C temperature for 30 minutes. Metallographic specimens were prepared in the normal way by mounting in resin, grinding on water-lubricated silicon carbide papers and polishing with diamond paste down to 1 μm finish. Phases of samples were identified by means of Rigaku Ultra IV XRD model diffractometer with Cu-Kα radiation (λ=1.5418 Å). The scan ranges from 10° to 90°, with a step size of 0.02° 2θ, and counting time of 0.5 s was applied at each step. The

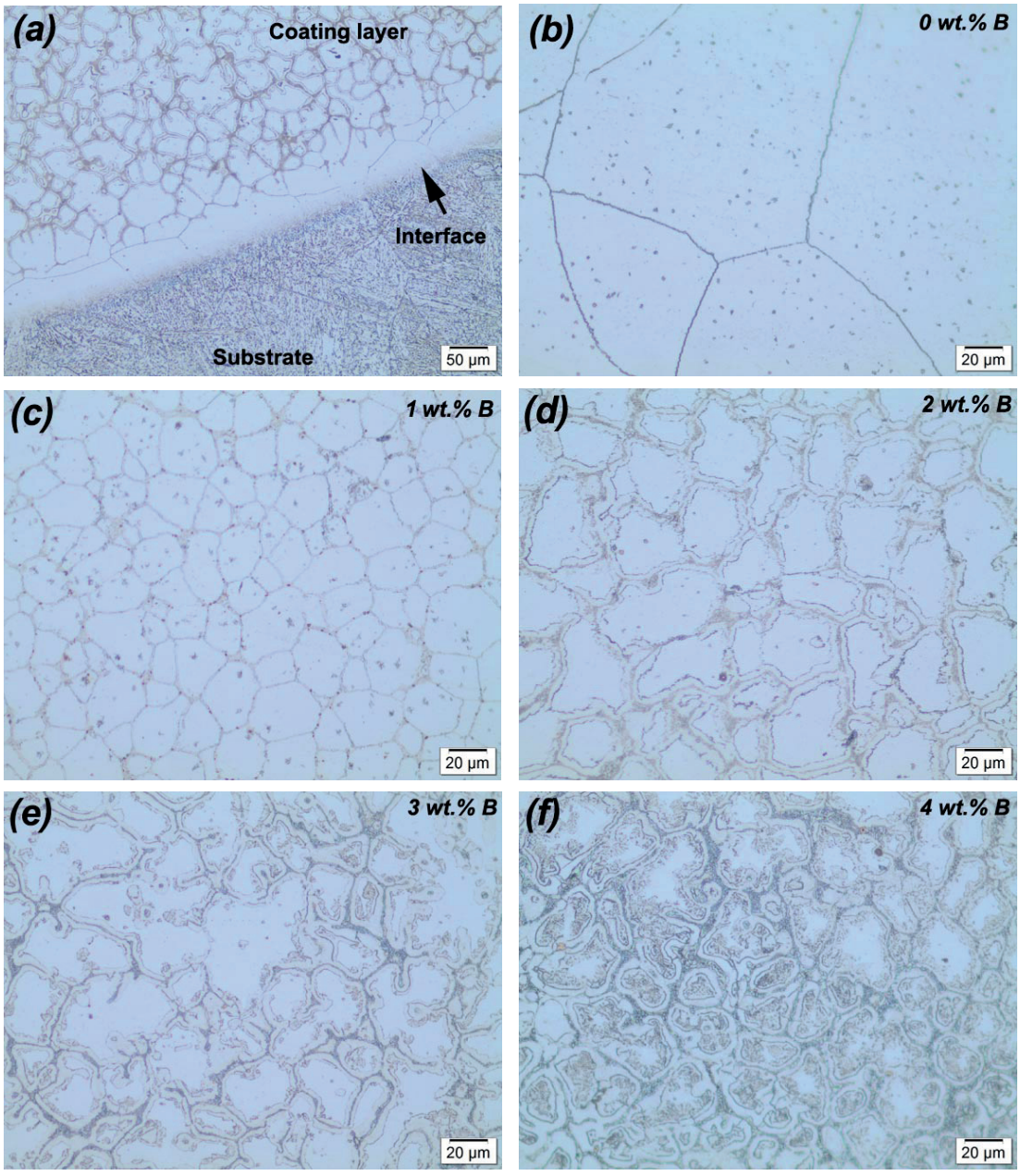

Fig. 2. Optic images of coatings: (a) general appearance, (b-f) changing appearance of coating layer depending on boron additives

morphologies of coatings were evaluated by SEM (Carl Zeiss Ultra Plus Gemini FESEM, Australia). Chemical composition of coatings was determined by means of energy dispersive spectrometry (EDS) in the SEM. Microhardness measurements were carried out by using Shimadzu HVM-2 model digital microhardness tester. The load was applied for 15 s and at 300 g.

3. Results and discussion

Optical photographs of Mo-Si-B-based coatings produced using TIG process are shown in Fig. 2. Fig. 1a from these photographs represents a general appearance coating layer-interface-substrate. According to Fig. 2a, a thin white layer was observed on the interface, which indicates good metallurgical bonding between the deposited coating and the substrate [11]. Figs. 2b-1f show the microstructure morphology of the coating layer depending on increasing boron rates. When the coating layers are examined, it is clear that the coating layers have crack/pore free and homogeneous structure. It is clearly seen that as the boron amount increased, grains in the coating layer were finer and it has been phase precipitation in the grain boundary. It is partly seen that this precipitation occurred also inside of grains. Considering the coatings made with TIG, it has shown that coating layer in the studies in the literature has a dendritic microstructure [12-14]. Unlike other studies, dendritic formation was not observed in this study. It has been considered that it is due to the precipitation of grain boundary which may prevent elongation of grains and low cooling rate. Grain boundaries in Mo-Si coating without boron are seen as a line, but it has been seen from Fig. 3 that this line occurred with the formation of the precipitated phases in the large magnification. Fig. 3 shows both map analysis and the EDS line of Mo-Si coating. It is clear that molybdenum is intense in the grain boundary. Also, iron dominated inside of grains. Iron amount decreased grain boundary. The amount of silicon is the same for both inside of grain and grain boundary.

With boron addition to Mo-Si coating, formation of different phases occurred grain boundary and this formation further expanded grain boundary line. Microstructural formation in the iron grain boundary was eutectic formation. In Mo-Si-B coatings, Fe, Si, and B occurred in both inside of grain and grain boundary while Mo formed in the grain boundary. This situation was observed from MAP analysis of Mo-Si-B coating in Fig. 4. SEM image and EDS analysis of the Mo-Si-3 wt.% B coating are shown in Fig. 5. Except for a small amount of primary Mo solid solution (Mo_{ss}) among the iron grains, there was a majority of two-phase eutectic microstructure and a small amount of three-phase microstructure between the eutectic areas. While two-phases eutectic microstructure was Mo_{ss}+Mo_5SiB_2, three-phase microstructure was Mo_{ss}+Mo_5SiB_2+Mo_3Si. Thanks to Mo_2B phase formed due to the presence of boron, these eutectic structures were finer. In Fig. 5, points 1 and 2 indicate Mo_2B phase; point 3 indicates Mo_5SiB_2 (T2) phase; point 4 indicates Mo_3Si (A15) phase and point 5 indicates Fess phase. The possibility of this phase was determined starting from the chemical composition of the EDS points and XRD graph in Fig. 6a.

Fig. 6a shows the X-ray diffraction (XRD) spectra of Mo-Si-B coatings. XRD analysis revealed the presence of α-Mo, α-Fe, Mo_3Si, Mo_2B and Mo_5SiB_2 phases. Theoretically, the possible products of the reaction among liquid Mo, Si and B may be Mo_3Si, Mo_2B and Mo_5SiB_2 according to the Mo-Si-B ternary phases diagrams (Fig. 6b). In this study, to form the Mo_3Si, Mo_2B and Mo_5SiB_2 phases, the point 1, 2, 3, 4 and 5 in the diagram in Fig. 6b

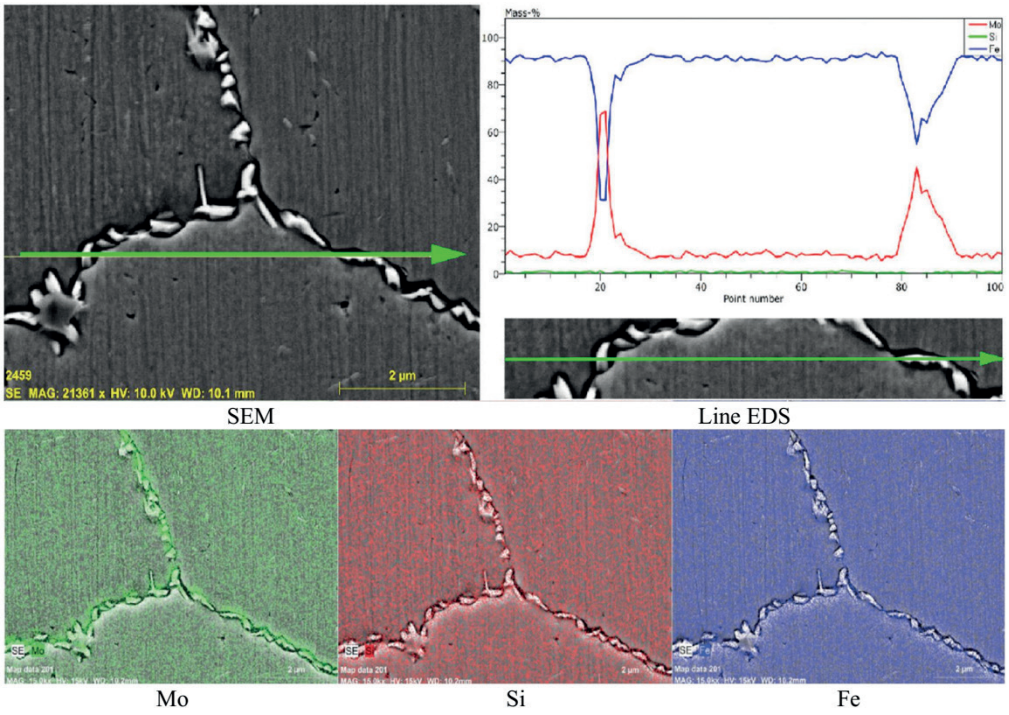

Fig. 3. Line EDS analysis and MAP analysis of the Mo-Si coating without boron

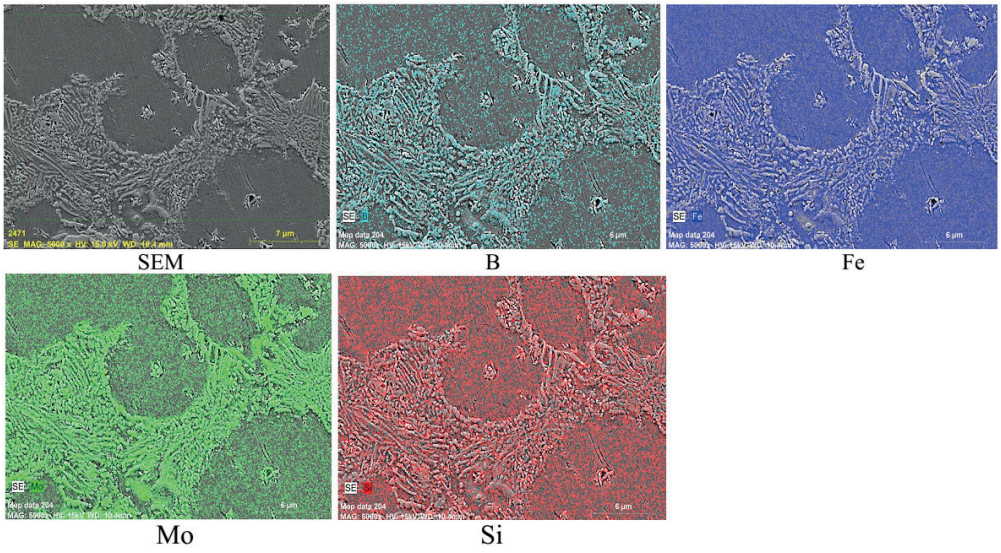

Fig. 4. MAP analysis of the Mo-Si-B coating (3 wt.% B)

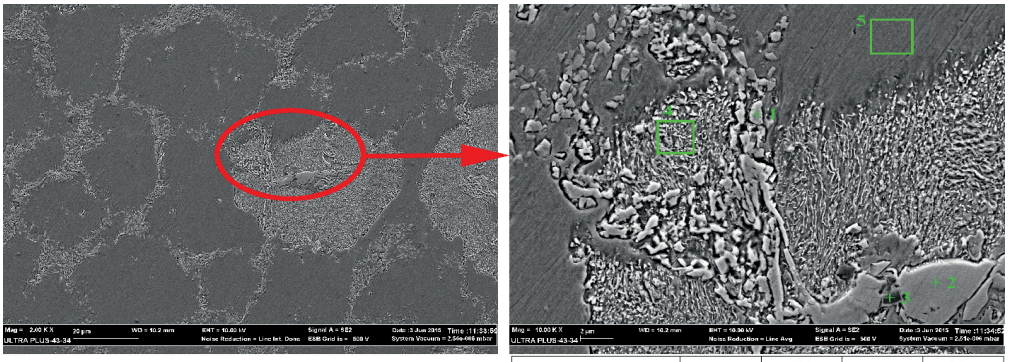

EDS point/area	Mo	Si	B	Fe
	at%	at%	at%	at%
1	28.11	0.42	40.35	31.11
2	23.93	1.50	51.32	23.25
3	65.25	13.50	16.50	4.75
4	46.15	6.45	11.85	35.55
5	8.71	2.10	8.92	80.26

Fig. 5. SEM image and EDS analysis of the Mo-Si-3 wt.% B coating

were already selected deliberately. According to the XRD pattern, the dominant phases in the microstructure are α-Mo and α-Fe. Iron phase comes from substrate. As increasing amount of boron, the intensity of the Mo_2B and Mo_5SiB_2 peak increased. It was observed that intensity of the Mo_3Si phase didn't change.

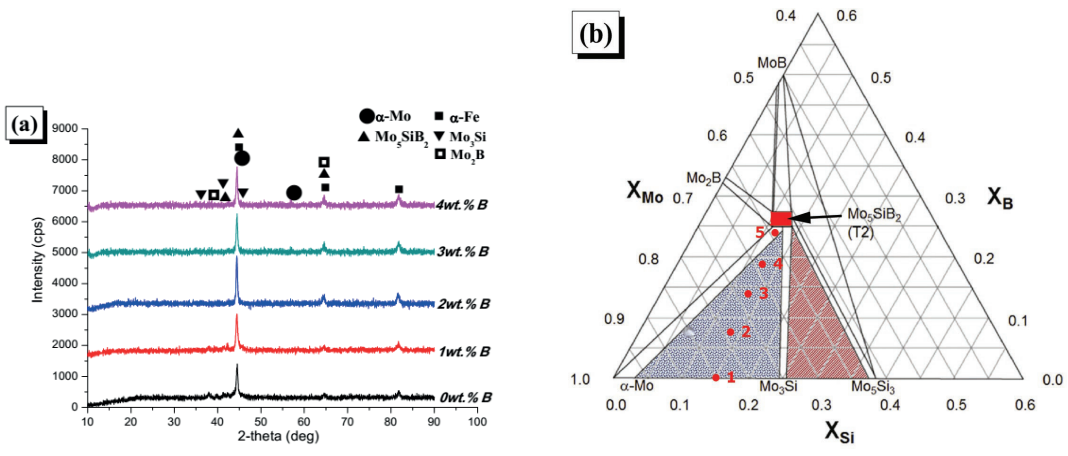

Fig. 6. (a) XRD graph of the Mo-Si-B coatings, (b) Mo-Si-B ternary phase diagram [15-18].

Fig. 7 shows the micro-hardness distribution ranging from substrate to the surface of the coatings. The average thickness of the coating is about 1.2 mm. Hardness measurements have been taken under 0.2 mm of coating surface. Microhardness increased with increasing amounts of boron. The average hardness values of the coating changed between 735 $HV_{0.3}$ and 1140 $HV_{0.3}$. The microhardness of the coating is higher than that of the substrate of 200 HV0.3. The reason for this can be attributed to the grain refinement and binary and ternary metallographic phases.

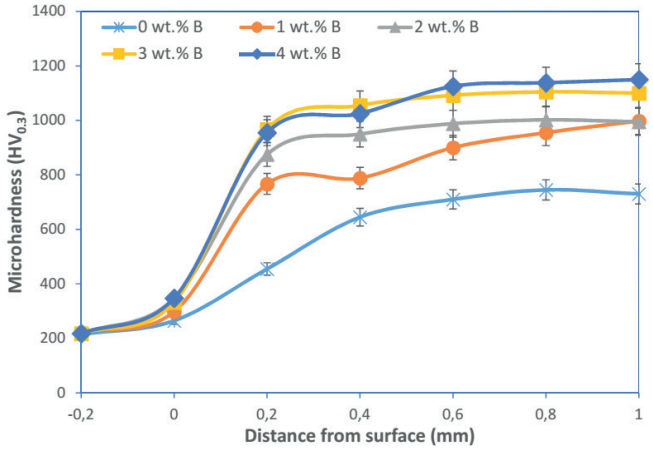

Fig. 7. Effect of boron content on Mo-Si-B coatings

4. Conclusions

This study aims to investigate microstructural changes in Mo-Si-B coating produced using tungsten inert gas (TIG) process. With this aim, boron amount was changed as 0 wt.%, 1 wt.%, 2 wt.%, 3 wt.% and 4 wt.%. SEM and optic images showed that the microstructure morphology of the coating layer changed depending on increasing boron rates and coating layers had crack/pore free and homogeneous structure. Besides, as the boron amount increased, grains in the coating layer were finer and precipitation in the grain boundary occured. XRD showed that microstructure consisted of α-Mo, α-Fe, Mo2B, Mo3Si and Mo5SiB2 phases. The hardness of coating was significantly improved with increasing boron content.

REFERENCES

[1] W.O. Soboyejo, T.S. Srivatsan, Advanced Structural Materials: Properties, Design Optimization, and Applications, Taylor & Francis, (2006).

[2] E.A. Levashov, Yu. S., Pogozhev, A. Yu., Potanin, N.A. Kochetov, D. Yu. Kovalev, N. V. Shvyndina, T. A. Sviridova, Ceramics International, **40**, 5, 6541 (2014).

[3] A.B. Gokhale, G.J. Abbaschian, J. Phase Equilibria, **12**, 493 (1991).

[4] J.H. Schneibel, R.O. Ritchie, J.J. Kruzic, P.F. Tortorelli, Intermetallic Alloys, **36a**, 531, (2005).

[5] K.S. Kumar, A.P. Alur, Division of Engineering, Brown University, 182 Hope Street, Providence, RI 02912, USA Available online (2006).

[6] M.K. Meyer, M. Akinc, Journal of the American Ceramic Society, **79**, 938, (1996).

[7] J.A. Lemberg, and R.O. Ritchie, Advanced Materials, **24**, 26, 3445, (2012).

[8] M. Krüger, S. Franz, H. Saage, M. Heilmaier, J.H. Schneibel, P. Jéhanno, M. Böning, H. Kestler, Intermetallics, **16**, 7, 933, (2008).

[9] S. Islak, O. Eski, S. Buytoz, Optoelectronics and Advanced Materials – Rapid Communications, **5**, 65, (2011).

[10] S. Islak, S. Buytoz, and M. Karagöz, Indian Journal of Engineering & Materials Sciences, **19**, 253, (2012).

[11] G. Azimi, and M. Shamanian, Journal of Alloys and Compounds, **505**, 2, 598, (2010).

[12] S.O. Yılmaz, Surface and Coatings Technology, **201**, 3, 1568, (2006).

[13] S. Buytoz, Surface and Coatings Technology, **200**, 12, 3734, (2006).

[14] G. Tosun, Arabian Journal for Science and Engineering, **39**, 3, 2097, (2014).

[15] M. Akinc, M.K. Meyer, M.J. Kramer, A.J. Thom, J.J. Huebsch, B. Cook, Materials Science and Engineering, **261**, 1-2, 16, (1999).

[16] M. Meyer, M. Kramer, M. Akinc, Advanced Materials, **8**, 1, 85, (1996).

[17] M.K. Meyer, A.J. Thom, M. Akinc, Intermetallics, **7**, 2, 153, (1999).

[18] D. Berczik, Method for enhancing the oxidation resistance of a molybdenum alloy, and a method of making molybdenum alloy, U.S. Patent Number **5**, 595-616, (1997).